



Characterization of zonal winds in the stratosphere of Titan with UVES: 2. Observations coordinated with the Huygens Probe entry

David Luz, T. Civeit, Régis Courtin, Jean-Pierre Lebreton, Daniel Gautier, Olivier Witasse, Andreas Kaufer, Francesca Ferri, Luisa M. Lara, Timothy A. Livengood, et al.

► To cite this version:

David Luz, T. Civeit, Régis Courtin, Jean-Pierre Lebreton, Daniel Gautier, et al.. Characterization of zonal winds in the stratosphere of Titan with UVES: 2. Observations coordinated with the Huygens Probe entry. Journal of Geophysical Research. Planets, 2006, 111, <10.1029/2005JE002617>. <hal-03786648>

HAL Id: hal-03786648

<https://hal.science/hal-03786648v1>

Submitted on 23 Sep 2022

HAL is a multi-disciplinary open access archive for the deposit and dissemination of scientific research documents, whether they are published or not. The documents may come from teaching and research institutions in France or abroad, or from public or private research centers.

L'archive ouverte pluridisciplinaire **HAL**, est destinée au dépôt et à la diffusion de documents scientifiques de niveau recherche, publiés ou non, émanant des établissements d'enseignement et de recherche français ou étrangers, des laboratoires publics ou privés.



Copyright - All rights reserved

Characterization of zonal winds in the stratosphere of Titan with UVES:

2. Observations coordinated with the Huygens

Probe entry

D. Luz,^{1,2} T. Civeit,³ R. Courtin,² J.-P. Lebreton,³ D. Gautier,² O. Witasse,³
A. Kaufer,⁴ F. Ferri,⁵ L. Lara,⁶ T. Livengood,⁷ and T. Kostiuk⁷

Received 21 October 2005; revised 28 March 2006; accepted 23 June 2006; published 23 August 2006.

[1] The Huygens Probe has successfully entered Titan's atmosphere and landed on its surface on 14 January 2005. With the aim of characterizing the zonal wind flow in Titan's stratosphere close to the time of entry, coordinated observations were carried out at the Very Large Telescope on the nights of 7, 12, 14, and 15 January. As in our previous investigation (Luz et al., 2005), we used the UVES instrument, mounted on the Kueyen-UT2 telescope, simultaneously achieving high spectral resolving power and high spatial resolution. The field has been derotated in order to align the 0.3-arcsec aperture perpendicularly to Titan's rotation axis. In this configuration, spatial information in the east-west direction is preserved in a set of spectra in the direction perpendicular to dispersion. We present measurements of zonal winds obtained with the technique of absolute accelerometry. The observations were made in the wavelength range 4200–6200 Å, probing between 115 and 280 km, with peak contributions at 200 and 170 km for the lower and upper parts of the domain. We detect prograde zonal winds with lower limits 46 and 53 ms⁻¹ at these altitudes. These values are close to our previous measurements.

Citation: Luz, D., et al. (2006), Characterization of zonal winds in the stratosphere of Titan with UVES: 2. Observations coordinated with the Huygens Probe entry, *J. Geophys. Res.*, *111*, E08S90, doi:10.1029/2005JE002617.

1. Introduction

[2] Saturn's giant moon, Titan, is the only satellite in the Solar System with a dense atmosphere. With a very close interaction between the photochemistry occurring in the high atmosphere, the formation and microphysics of aerosol particulates, a full methane cycle similar to the terrestrial hydrological cycle, and atmospheric dynamics, Titan is a rich meteorological system. Dynamically, its rotation regime is intermediate between the fast 24 hour period of the Earth and the 243 days of Venus. These characteristics make it one of the most interesting bodies of the Solar System and a good subject for comparative planetology.

[3] Since February 2002, Titan has been observed by our team at the Very Large Telescope in Paranal with the UVES

instrument. The objective was to measure the winds in the stratosphere, using the method of absolute accelerometry of Connes [1985]. The feasibility of the experiment had been tested previously with Venus observations at the Observatoire de Haute Provence [Martić et al., 2001]. With the Cassini-Huygens Saturn orbit insertion planned for July 2004, we decided in June 2003 to propose new observations coordinated with the Huygens Probe Mission [Lebreton and Matson, 1997], which occurred on 14 January 2005.

[4] Here we present and discuss observations made on 8, 13, 15, and 16 January. The results of the observations made in 2002 and 2003, as well as the method and data processing used, have been presented in two previous articles (Luz et al. [2005], hereinafter cited as paper 1, and Civeit et al. [2005]). The reader is referred to these works for details on the type of observations and method. This study was carried out in the framework of coordinated observations between the Huygens Mission and ground-based observers, in particular with the wind measurements by Kostiuk et al. [2006], this issue using the HIPWAC instrument.

2. Observations

[5] Table 1 summarizes the observations and Figure 1 presents a scheme of the observation geometry. The observations were made in UVES service mode. They probe Titan's atmosphere in the 4200–6200 Å region, and use the

¹Centro de Astronomia e Astrofísica da Universidade de Lisboa (CAAUL), Observatório Astronómico de Lisboa, Lisbon, Portugal.

²Laboratoire d'Etudes Spatiales et d'Instrumentation en Astrophysique (LESIA), Observatoire de Paris, Paris, France.

³Research and Scientific Support Department of ESA, ESTEC, Noordwijk, Netherlands.

⁴European Southern Observatory, Santiago, Chile.

⁵CISAS/Università di Padova, Padova, Italy.

⁶Instituto de Astrofísica de Andalucía/CSIC, Granada, Spain.

⁷NASA Goddard Space Flight Center, Greenbelt, Maryland, USA.

Table 1. Log of the Titan Observations^a

Exposure	Date (yy-mm-dd)	Time UT (hh:ss)	Air Mass	Seeing, ''	ϵ_{EEV}	ϵ_{MIT}	Region
1	05-01-08	04:45	1.45	0.82	1.39	1.59	Eq
2	05-01-08	04:54	1.44	0.75	1.44	1.36	Eq
3	05-01-08	05:06	1.43	0.53	1.41	1.73	Eq
4	05-01-08	05:15	1.43	0.89	1.42	1.38	Eq
5	05-01-08	05:32	1.44	0.74	1.22	0.79	Eq
6	05-01-08	05:41	1.45	0.74	1.24	0.93	Eq
7	05-01-08	05:53	1.46	0.80	0.90	0.43	Eq
8	05-01-08	06:02	1.48	0.72	0.98	1.01	Eq
9	05-01-13	04:57	1.44	0.69	1.13	0.26	Eq
10	05-01-13	05:27	1.46	0.73	1.28	2.08	Eq
11	05-01-13	05:36	1.48	0.74	1.77	1.82	N
12	05-01-13	05:46	1.49	0.66	0.71	0.36	S
13	05-01-13	06:00	1.53	0.65	1.19	0.41	Eq
14	05-01-13	06:10	1.55	0.66	1.49	0.90	N
15	05-01-13	06:19	1.58	0.68	0.35	0.26	S
16	05-01-15	05:20	1.46	0.88	1.11	1.27	Eq
17	05-01-15	05:29	1.48	0.78	1.76	1.26	Eq
18	05-01-15	05:41	1.50	0.69	0.74	0.75	Eq
19	05-01-15	05:50	1.52	0.86	1.49	1.32	Eq
20	05-01-15	06:07	1.57	0.89	1.25	1.42	Eq
21	05-01-15	06:16	1.61	0.80	1.09	1.34	Eq
22	05-01-15	06:27	1.65	0.74	1.19	1.60	Eq
23	05-01-15	06:36	1.70	0.82	1.11	0.81	Eq
24	05-01-16	05:00	1.45	0.58	0.52	0.40	Eq
25	05-01-16	05:09	1.46	0.73	0.45	0.24	Eq
26	05-01-16	05:21	1.47	0.71	0.42	0.34	Eq
27	05-01-16	05:30	1.49	0.71	0.22	0.51	Eq
28	05-01-16	05:46	1.53	0.89	1.01	0.92	Eq
29	05-01-16	05:56	1.55	0.91	0.78	0.79	Eq
30	05-01-16	06:07	1.59	0.93	0.63	0.85	Eq
31	05-01-16	06:16	1.62	0.68	0.70	0.48	Eq
32	05-01-16	06:32	1.70	0.61	0.70	0.65	Eq

^aThe seeing is indicated as measured by the differential image motion monitor at Paranal. Different observation blocks are separated by empty rows. The derotator position angle is set to 83.3 degrees (aperture perpendicular to spin axis). Three regions are defined: equator (Eq), north (N), and south (S), with the aperture centered at 0, +0.22 arcsec, and −0.22 arcsec, respectively, relative to the subterrestrial point. Titan's radius was 0.44 arcsec at the time of the observations. The air mass is defined as $1/\cos z$, z being the zenith angle.

same settings as the ones described in paper 1, except for the following three points.

[6] First, here the derotator was fixed at a position angle of 83.3°, which still corresponds to an alignment of the aperture perpendicularly to the spin axis of Titan, but with the same side of the slit corresponding always to the same hemisphere of Titan (eastern or western). In our previous observations (see paper 1) we have encountered unexpected large variations in our measurements in a very short time scale (night of 12 December 2003), which may have been related to changes in the derotator orientation between observation blocks. By keeping the derotator at a fixed angle, in this work we have tried to eliminate that source of uncertainty.

[7] Second, here we allowed a maximum seeing of 0.8 arcsec, instead of 0.6, to maximize the probability of obtaining data within a narrow time frame around the entry date of 14 January. Ideally, for an object as small as Titan the observations should be made with a seeing as low as possible. However, this objective is difficult to achieve. The

mean seeing has increased at the Paranal site since the construction of the Very Large Telescope (VLT) (from about 0.7 to 0.9 arcsec (see <http://www.eso.org/gen-fac/pubs/astclim/paranal/seeing/singstory.html>), and seeings less than 0.5 arcsec only occur about 7–9% of the time (see <http://www.eso.org/gen-fac/pubs/astclim/paranal/seeing/seewind>)).

[8] Third, in two observation blocks we allowed for exposures centered in the northern and southern hemispheres of Titan's disk, in order to explore latitudinal variations of the winds. Both pre-Cassini observations [Flasar *et al.*, 1981; Hubbard *et al.*, 1993; Bouchez, 2004] and models [Hourdin *et al.*, 1995, 2004] pointed to large latitudinal variations, on the order of 100 ms^{-1} between the stratospheric winter jet and the equator. Due to the limited telescope time available, we restricted these off-center observations to two blocks. The three rectangles and circles in Figure 1 show the slit positions in these exposures. The central point was done first, subsequently

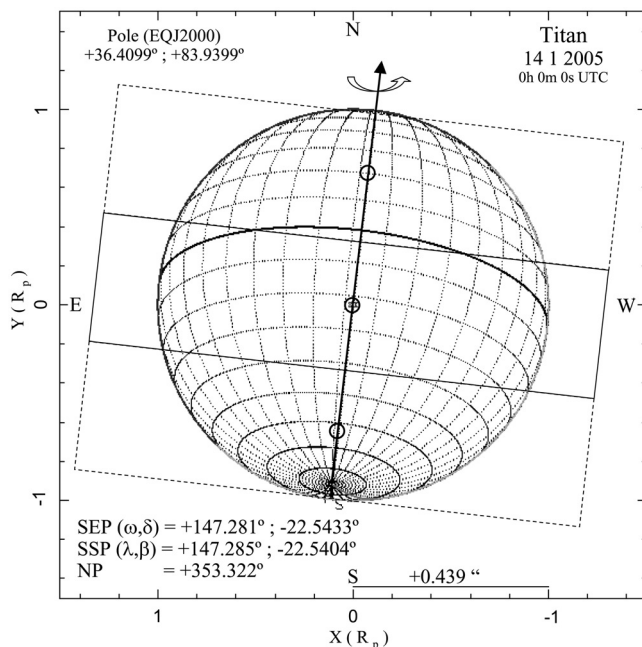


Figure 1. Observing geometry at 14 January 2005. Titan’s diameter is ~ 0.88 arcsec, and the slit width is 0.3 arcsec. X and Y are in units of Titan radii. The slit length of 8.9 arcsec is not shown to scale. Dashed rectangles indicate the slit positions for the exposures centered in the northern and southern hemispheres. The figure shows the celestial east and west directions.

shifting to north and south (marked respectively Eq, N and S in Table 1).

3. Results

[9] The UVES echellograms are recorded in a mosaic of two CCDs, one EEV and one MIT CCD chips that register respectively the lower- and upper-wavelength parts of the spectrum, respectively 4200–5200 Å (29 spectral orders) and 5200–6200 Å (18 orders). The region of the atmosphere probed has been determined by radiative transfer modeling to be between 115 and 280 km (Figure 10b in paper 1), with peak contributions at 200 and 170 km for the EEV and MIT branches, respectively. Orders corresponding to the EEV and MIT CCD chips are treated separately. The Doppler shifts are computed for each order and for each spatial position relative to the slit center using the technique of *Connes* [1985], as implemented by *Civeit et al.* [2005]. After bias and background subtraction and flat-fielding, order center locations are mapped and 2-D spectral orders are extracted. The extraction window is 31 pixels and the pixel scale is 0.18 pixels, making Titan’s diameter about 5 pixels. To avoid spurious features arising from the discrete nature of the CCD pixel matrix, and to match the center of the extracted 2-D profile with the center of the disk, the extracted 2-D orders are interpolated and recentered. Wavelength calibration, and the correction for the error induced by slit image curvature on the velocity measurements, are done on the basis of Thorium-Argon lamp exposures which have been included in observation blocks.

[10] Figures 2–5 show the velocity curves extracted from the spectra. Curves from individual orders are shown as the blue and red dotted lines, and correspond respectively to the EEV and MIT CCDs. The 31 pixels in abscissa correspond to the full width of the 2-D extraction window, and there are 29 curves for the lower part of the spectrum and 18 curves for the upper part (one for each order). The mean-weighted sums, computed from the ensemble of order curves for each CCD chip, are shown as the solid blue and red lines. Pixels are measured relative to the centroid of the intensity distribution in the echelle order. Titan east (i.e., celestial west) is to the left, indicating prograde winds in most curves (i.e., positive Doppler shift).

[11] From the velocity curve we extract the mean equatorial velocity. The extraction is based on the symmetry of the curve: the point of symmetry of the weighted sum curve is first computed using a least-squares fit, and a central domain is determined where the Doppler shifts from opposite symmetrical points in the disk coincide to within a tolerance of 5σ . Nonsymmetric regions of the curve (i.e., Doppler shifts differing by more than 5σ) are rejected as spurious. The maximum shift velocity within the radius of symmetry is taken as the best approximation to the true velocity. This value has to be divided by $2 \cos \alpha$ to account for the double Doppler shift induced by backscattering and for the projection of the zonal wind component, which depends on the obliquity α . Finally, surface rotation is subtracted in order to obtain the wind velocity relative to the surface (see paper 1).

[12] Figure 6 shows the measurements retrieved from the velocity curves, applying this technique. Figure 6a shows only results for the equatorial region (exposures 11, 12, 14 and 15 probe the northern and southern regions and were left out). The Huygens entry occurred between exposures 15 and 16. Figure 7 shows the measurements for the two observation blocks that probed the northern and southern hemisphere (exposures 10–15).

[13] The results are similar to those from our previous series of observations (paper 1). Most of the velocity curves indicate prograde winds, with a large variability of the magnitudes of the Doppler shift maxima. A fraction of the curves indicate retrograde winds. Many curves are also flat in the central part of the disk and/or exhibit asymmetries relative to the center. There are, however, the following differences:

[14] 1. Less variability, which is probably related to better tracking. In this observing run we submitted better ephemeris data for telescope guiding than for previous observations. In principle, this is not important, since secondary guiding at the VLT should always keep the source on the aperture. However, it is possible that an extended source such as Titan poses an additional difficulty to the guiding algorithm. In our case, the precaution seems to have been fruitful.

[15] 2. A smaller fraction of retrograde measurements. In Figure 6a, exposures 24 and 27, lower branch, and 9 and 27, upper branch, are below 0 by more than 1σ (compare with Figure 8a of paper 1). All retrogrades obtained for observations with the aperture placed at the equator are above -11.7 ms^{-1} . This is the value one obtains after subtracting the surface rotation from a flat velocity curve. These retrograde measurements can simply be interpreted as false

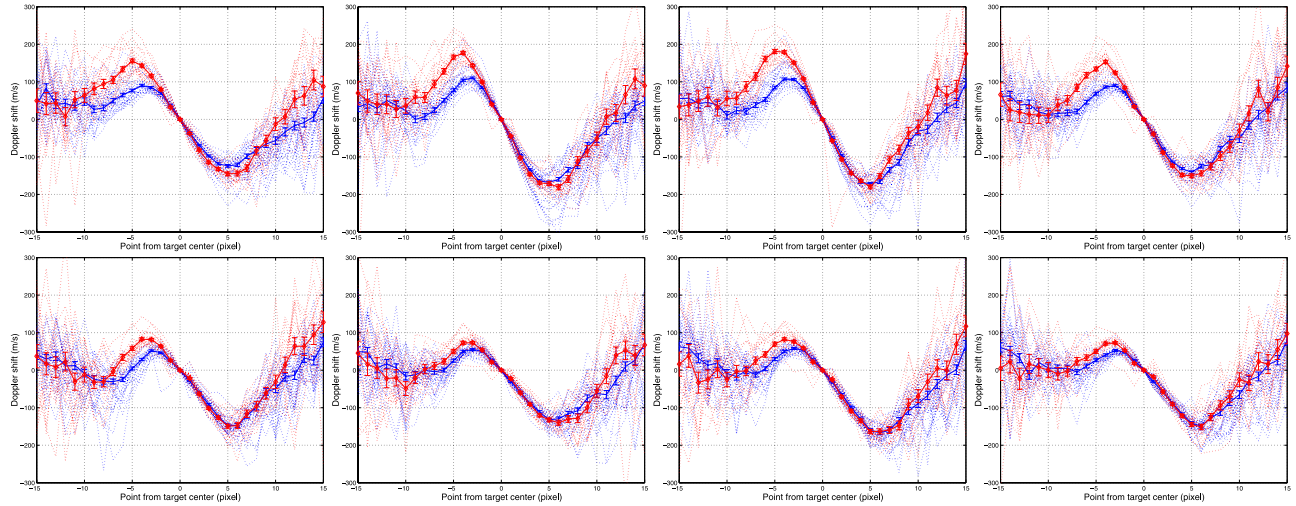


Figure 2. Velocity curves for exposures 1–4 (top, left to right) and 5–8 (bottom, left to right) from Table 1. Order velocity curves from the EEV (blue) and MIT (red) CCDs are shown as dotted lines. The weighted sums of order curves are shown as the two solid lines. Titan east is to the left, and the positive Doppler shift there indicates the atmosphere is receding. The velocities are shown prior to correction for the double Doppler shift induced by backscattering, axis tilt, and surface rotation.

retrogrades that arise from correcting velocity curves that are essentially flat. They arise from high-seeing exposures, in which turbulence in the terrestrial atmosphere degrades spatial resolution to a point where the eastern and western hemispheres become indistinguishable.

[16] 3. A more sensible variation of measured velocities with the quality factor, with less dispersion. The quality factor is defined as $\varepsilon = R_s/R_{eff}$, where R_s is the radius of symmetry of the velocity curve and R_{eff} is the effective radius, defined as the mean half width of the extracted orders. This quality factor can be used as a measure of the global quality of the observations. Exposures obtained at high seeing conditions, which seriously flattens the velocity

curve, have their order width enlarged. On the other hand, a symmetric curve indicates that the target stayed centered throughout the exposure. The running average shown in Figure 6b reaches a maximum at $\varepsilon = 1.375$, with $\overline{V_{EEV}} = 46.3 \pm 7.5 \text{ ms}^{-1}$ and $\overline{V_{MIT}} = 53.3 \pm 10.7 \text{ ms}^{-1}$, for the lower and upper part of the wavelength range. Since the accuracy of our method is limited, these measurements are interpreted as lower limits to the equatorial zonal wind velocity close to the Huygens Probe entry.

[17] 4. Unlike our previous observations, measurements in the upper wavelength region (MIT CCD) do not indicate weaker winds than for lower wavelengths (EEV CCD chip). The statistical tests described in paper 1 do not point to a

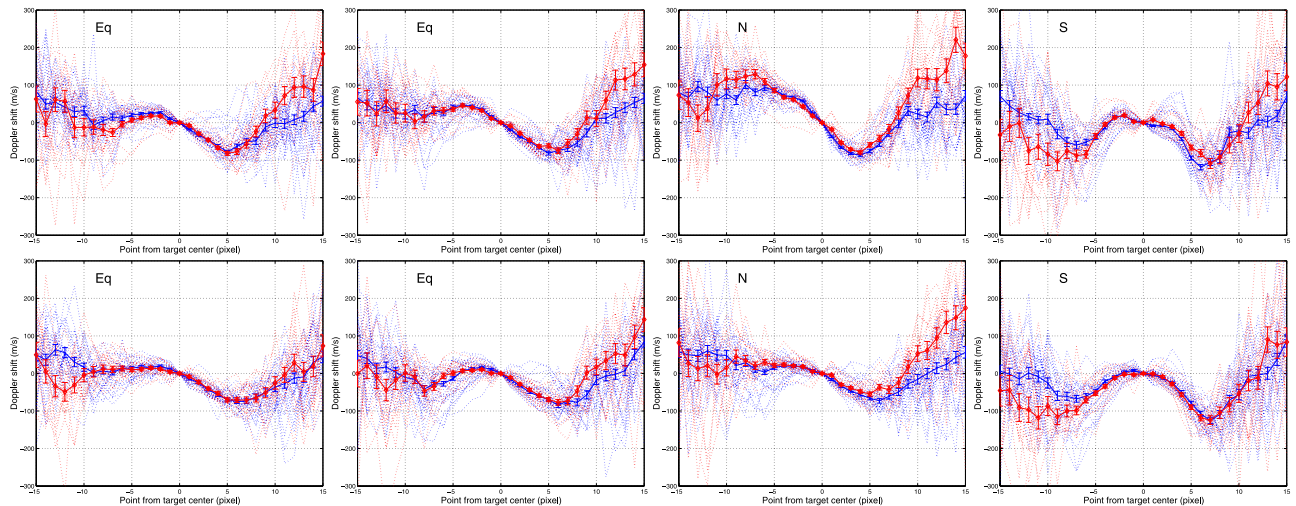


Figure 3. Same as Figure 2 for exposures 9–12 (top, left to right), 32, and 13–15 (bottom, left to right). Here the two exposures on the right in each row correspond to the northern and southern hemispheres, respectively. Exposure 32 (bottom left) is from a different night but is included here to facilitate layout.

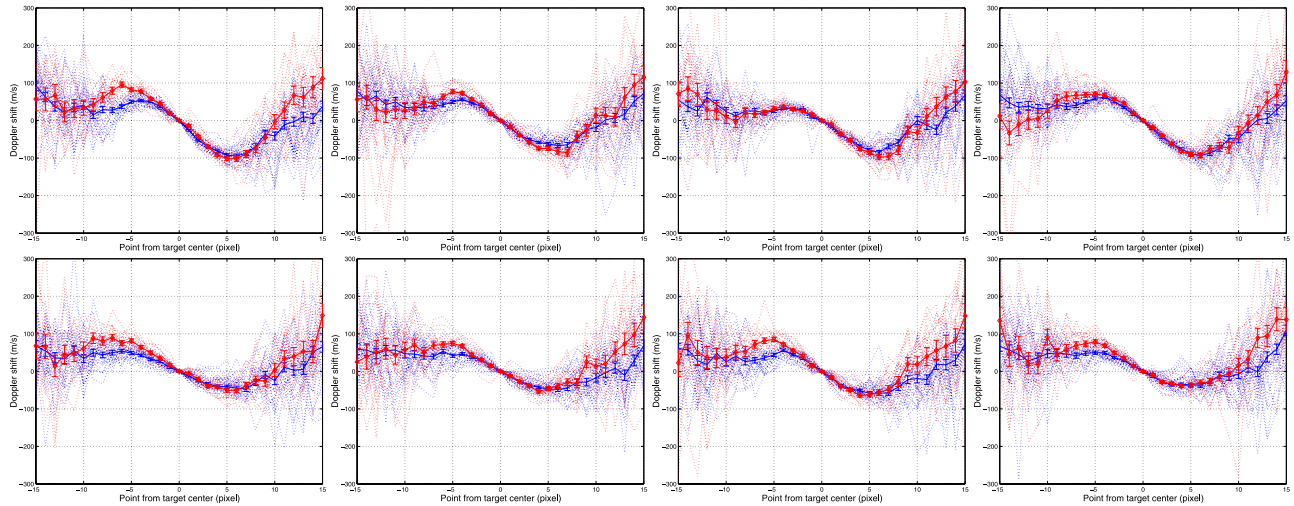


Figure 4. Same as Figure 2 for exposures 16–19 (top, left to right) and 20–23 (bottom, left to right).

significant difference between the two data sets. The Wilcoxon test statistic [Wilcoxon, 1945] corresponds to a probability $P_w \simeq 0.50$, which does not allow to reject the null hypothesis that the two distributions are identical. The paired t-test [e.g., Conover, 1999, p. 363], yields a consistent result.

[18] 5. The two observation blocks corresponding to the equator-north-south sequence are qualitatively consistent in their relative amplitudes, with winds increasing from south to north (Figure 7). The velocity curves for the southern hemisphere are almost flat, which indicates that the difference between the Doppler shifts at the eastern and western hemispheres is too small to compensate for the flattening due to the seeing. Once the correction for viewing angle and surface rotation is applied, these curves lead to false retrograde measurements close to -11.7 ms^{-1} . The mean relative increase in the Doppler shifts (corrected for geometry and surface rotation) between the equatorial and northern region is 65%. This is an estimate computed from the

two blocks of off-center observations, as $0.5 \times ((U_1^N - U_1^E)/U_1^E + (U_2^N - U_2^E)/U_2^E)$, where U_1^E and U_1^N are the mean Doppler shifts measured at the equator and at the northern hemisphere in the first block, respectively, and U_2^E and U_2^N are the same quantities for the second block. The mean Doppler shifts were computed as the means of the two CCDs. Although these measurements are lower limits of the zonal winds, it is useful to note that this estimate of the latitudinal variation is consistent with an increase from south to north, as expected for a wind profile typical of southern summer. Modeling and occultation observations yield a relative variation on the order of 50% [Hourdin *et al.*, 2004, Figure 2b; Sicardy *et al.*, 2006]. Due to the little data available, this estimate is only tentative. It assumes that relative measurements between two consecutive exposures are better than absolute measurements between exposure 10 and 13, because the probability of a large variation of the

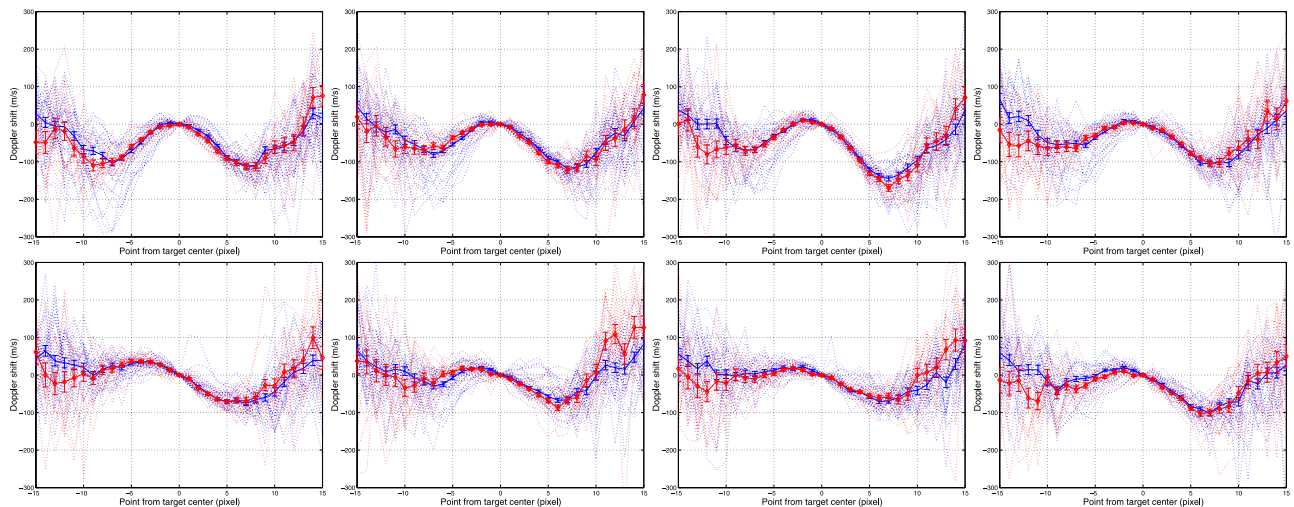


Figure 5. Same as Figure 2 for exposures 24–27 and 28–31.

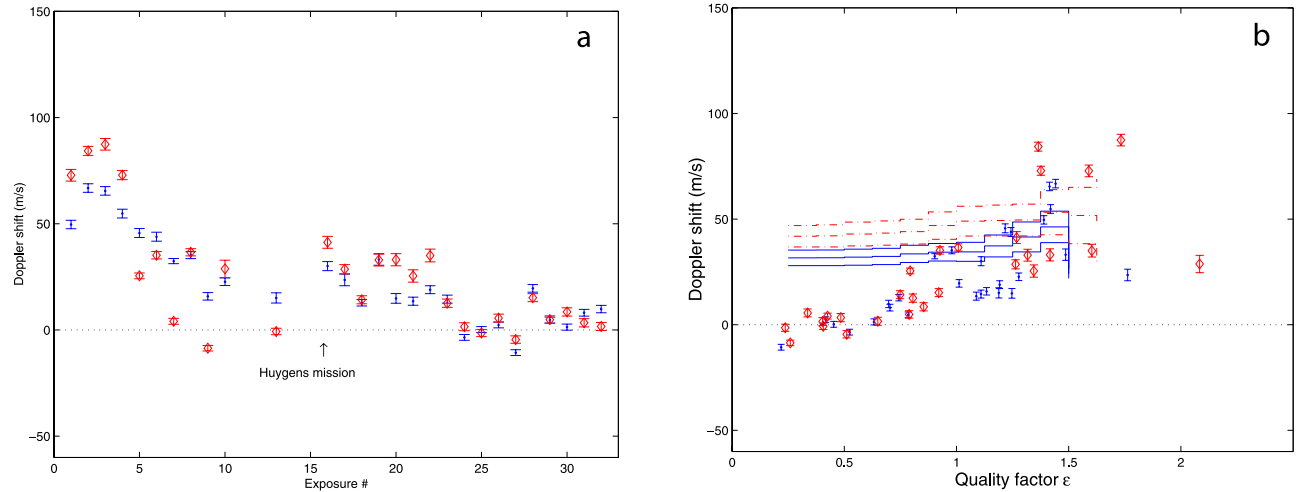


Figure 6. (a) Best estimate of the zonal wind velocity at the limb for the EEV (dots) and MIT (diamonds) CCD. The dotted line indicates null winds relative to the surface. The values shown have been corrected for the double Doppler shift, axis tilt, and surface rotation. Only exposures pertaining to the equatorial region are shown. (b) Same as Figure 6a, with measurements plotted as a function of the quality factor ϵ . The quality factor $\epsilon = R_s/R_{eff}$ can be used as a measure of the global quality of the observations, where R_s is the radius of symmetry of the velocity curve and R_{eff} is the effective radius, defined as the mean half width of the extracted orders. The central lines of each stair-step set of lines are running weighted averages for $\epsilon > \epsilon_0$ (solid line, EEV; dash-dotted, MIT CCD, step of 0.125 in ϵ) with the upper and lower lines at the $\pm\sigma$ positions. ϵ_0 can be read in abscissa. The two blocks including off-center exposures have not been included in either panel.

seeing (and eventually other conditions affecting the exposure) is smaller for consecutive exposures.

4. Discussion

[19] A variety of methods have been used in the past to measure the zonal winds in Titan's atmosphere. Figure 8a summarizes the most recent measurements, including this work and our previous measurements from paper 1.

[20] In the troposphere, clouds provide direct tracers for tracking, but their use for wind measurements before Cassini has been very limited. From integrated disk observations, clouds have been known to exist for almost a decade [Griffith *et al.*, 1998]. They were observed directly with adaptive optics imaging techniques [Brown *et al.*, 2002; Roe *et al.*, 2002; Bouchez and Brown, 2005], but the data set of cloud positions is too sparse to allow direct wind measurements. Long-term observations place an upper limit of 2.0 ms^{-1} eastward at $72\text{--}83^\circ$ south, at altitudes 10–20 km [Bouchez and Brown, 2005]. If a solid body rotation wind profile is assumed, which is a fair approximation for the summer hemisphere, this amounts to an upper limit of 16 ms^{-1} at the equator. Transient brightness variations detected in different positions close to the south pole have also been identified as clouds, possibly belonging to a varying extended weather system [Hirtzig *et al.*, 2006], but motion cannot be inferred directly.

[21] The Cassini Imaging Science Subsystem (ISS) observations are consistent with ground-based results. ISS detected clouds mainly at circumpolar southern latitudes,

with slow eastward motions which, extrapolated to the equator under the assumption of solid-body atmospheric rotation, yield a zonal wind of $19 \pm 15 \text{ ms}^{-1}$ [Porco *et al.*, 2005].

[22] The majority of wind measurements have concentrated on the stratosphere, where the zonal circulation is strongest. Historically, winds have been derived from the Voyager IRIS observations of temperature contrasts [Flasar *et al.*, 1981; Flasar and Conrath, 1990], from the atmospheric bulge observed during stellar occultations [Sicardy *et al.*, 1990; Hubbard *et al.*, 1993; Bouchez, 2004; Sicardy *et al.*, 2006] and were directly measured from the Doppler shifts of ethane lines in the infrared [Kostiuk *et al.*, 2001, 2004, 2005, 2006], of nitrile lines at millimeter wavelengths [Moreno *et al.*, 2005] and of Fraunhofer solar absorption lines in the visible [Luz *et al.*, 2005; this work].

[23] In the lower stratosphere and troposphere, ground-truth measurements by the Doppler Wind Experiment (DWE) onboard the Huygens Probe show first a marked decrease of zonal wind with altitude, from 100 ms^{-1} at 140 km to zero at 80 km, then an increase to 40 ms^{-1} at 60 km, before decreasing again to null zonal velocity at the surface [Bird *et al.*, 2005]. The LMD general circulation model (GCM) (from a database available at <http://www.lmd.jussieu.fr/titanDbase/index.html> [Rannou *et al.*, 2005]) reproduces qualitatively the measurements in the upper stratosphere, but seems to underestimate the winds there. The model prediction for January 2005 follows qualitatively the DWE profile, with one local maximum and one local minimum located close to the tropopause. In the model,

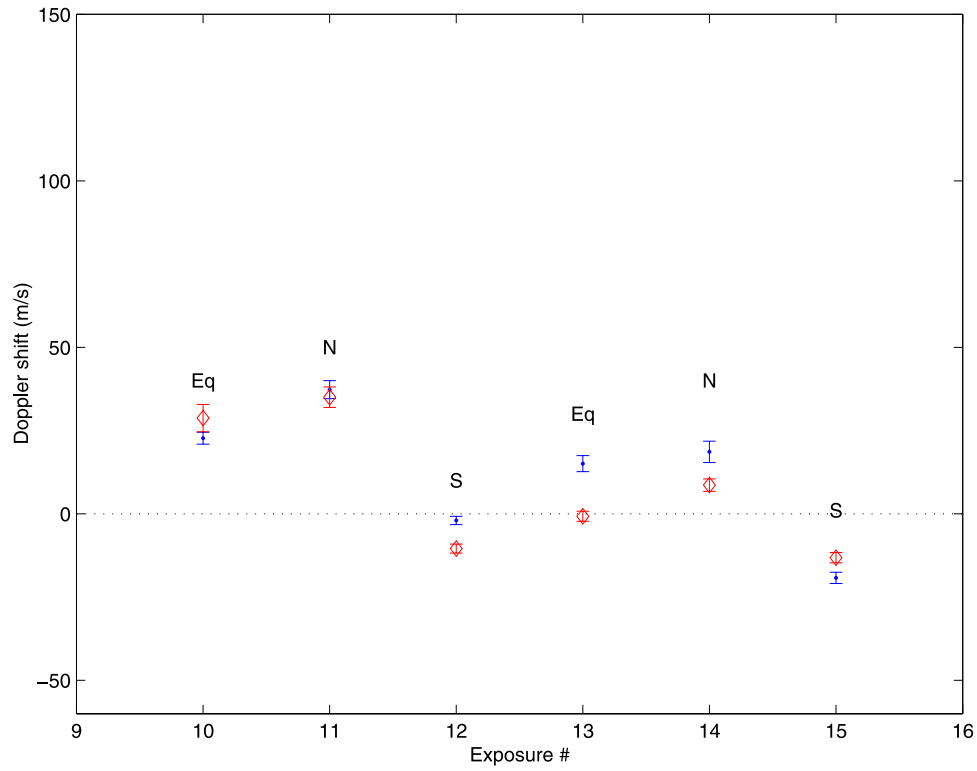


Figure 7. Same as Figure 6a, for the two observation blocks observing sequentially the regions Eq-N-S (exposures 10–15).

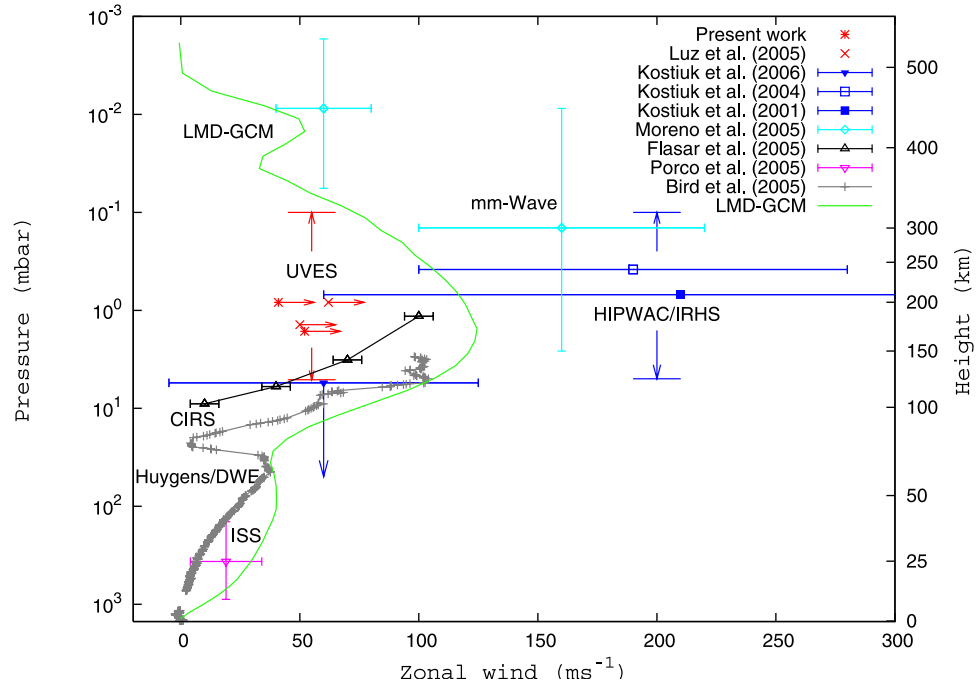


Figure 8. Comparison of wind measurements obtained with different techniques: absolute accelerometry in the visible [Luz *et al.*, 2005; this work], IRHS [Kostiuk *et al.*, 2001, 2004, 2006], millimeter observations [Moreno *et al.*, 2005], Cassini/CIRS [Flasar *et al.*, 2005], ISS [Porco *et al.*, 2005], and Huygens/DWE [Bird *et al.*, 2005] measurements. A prediction with the LMD-GCM for $L_s = 301^\circ$ has been included for comparison. The model results were taken from the Titan LMD-GCM database [Rannou *et al.*, 2005]. The UVES point at 170 km from Luz *et al.* [2005] has been slightly displaced upward for clarity.

the minimum is located close to 30 mbar, a region where the tropospheric and stratospheric Hadley cells are tangent [Luz *et al.*, 2003]. The measured wind shear between the two extrema is a factor of two higher than predicted, which may indicate that the model falls short of reproducing the latitudinal temperature contrast. The CIRS wind values in the lower troposphere [Flasar *et al.*, 2005] are also lower than the DWE profile. This could indicate a temporal variation in wind velocity, and the heights and velocities at the local extrema may be variable. However, since the CIRS retrieval is based on the integration of the thermal wind equation assuming null winds at 10 mb, it is possible that the CIRS winds are underestimated at low altitudes in the southern hemisphere. As pointed out by Flasar *et al.* [2005, supporting material], the correction to the retrieved wind solution, u_0 , due to a nonzero wind at 10 mb is of the order of $(u(10 \text{ mb})/u_0)^2$, making the correction small above ~ 2 mb.

[24] The UVES measurements consist of a highly scattered data set. The weighted average of our best measurements made in 2002 and 2003 placed lower limits of 50 and 62 ms^{-1} at 170 and 200 km altitude. The present work places somewhat lower limits, but the difference between the two altitudes probed is not significant statistically, as discussed above. Since we interpret these measurements as lower limits, it is not possible to conclude for a variation of the equatorial wind relative to our previous observations. It will be interesting, nevertheless, to await new wind measurements from Cassini to see if variations do occur. Titan's southern summer solstice was in October 2002, and northern spring equinox will occur in 2010, but model simulations suggest that changes in the atmospheric dynamics occur rapidly, rather than gradually [cf. Luz *et al.*, 2003, Figure 14]. A decrease is expected at low latitudes shortly after solstice, a prediction that Cassini will be able to test thoroughly in the coming years.

[25] **Acknowledgments.** The present article is based on observations collected at the European Southern Observatory, Chile, programme 074.C-0569(A). The authors are grateful to M. Bird for kindly providing the Huygens DWE wind measurements in electronic format and to F. Patat (ESO) for technical support. Figure 1 has been adapted from the IMCCE server (Institut de Mécanique Céleste et de Calcul des Éphémérides, <http://www.imcce.fr>). D. Luz acknowledges financial support from Fundação para a Ciência e a Tecnologia, Portugal (fellowship PRAXIS XXI/BPD/3630/2000 and project POCI/CTE-AST/57655/2004).

References

- Bird, M., et al. (2005), The vertical profile of winds on Titan, *Nature*, **438**, 800–802, doi:10.1038/nature04060.
- Bouchez, A. H. (2004), Seasonal trends in Titan's atmosphere: Haze, winds and clouds, Ph.D. thesis, chap. 4, Calif. Inst. of Technol., Pasadena.
- Bouchez, A. H., and M. E. Brown (2005), Statistics of Titan's south polar tropospheric clouds, *Astrophys. J.*, **618**, L53–L56, doi:10.1086/427693.
- Brown, M. E., A. H. Bouchez, and C. A. Griffith (2002), Direct detection of variable tropospheric clouds near Titan's south pole, *Nature*, **420**, 795–797.
- Civeit, T., T. Appourchaux, J.-P. Lebreton, D. Luz, R. Courtin, C. Neiner, O. Witasse, and D. Gautier (2005), On measuring planetary winds using high-resolution spectroscopy in visible wavelengths, *Astron. Astrophys.*, **431**, 1157–1166.
- Connes, P. (1985), Absolute astronomical accelerometry, *Astrophys. Space Sci.*, **110**, 211–255.
- Conover, W. J. (1999), *Practical Non-parametric Statistics*, 3rd ed., John Wiley, Hoboken, N. J.
- Flasar, F. M., and B. J. Conrath (1990), Titan's stratospheric temperatures: A case for dynamical inertia, *Icarus*, **85**, 346–354.
- Flasar, F. M., R. E. Samuelson, and B. J. Conrath (1981), Titan's atmosphere: Temperature and dynamics, *Nature*, **292**, 693–698.
- Flasar, F. M., et al. (2005), Titan's atmospheric temperatures, winds, and composition, *Science*, **308**, 975–978.
- Griffith, C. A., T. Owen, G. A. Miller, and T. Geballe (1998), Transient clouds in Titan's lower atmosphere., *Nature*, **395**, 575–578.
- Hirtzig, M., A. Coustenis, E. Gendron, P. Drossart, A. Negrão, M. Combes, O. Lai, P. Rannou, S. Lebonnois, and D. Luz (2006), Monitoring atmospheric phenomena on Titan, *Astron. Astrophys.*, in press.
- Hourdin, F., O. Talagrand, R. Sadourmy, R. Courtin, D. Gautier, and C. P. McKay (1995), Numerical simulation of the general circulation of the atmosphere of Titan, *Icarus*, **117**, 358–374.
- Hourdin, F., S. Lebonnois, D. Luz, and P. Rannou (2004), Titan's stratospheric composition driven by condensation and dynamics, *J. Geophys. Res.*, **109**, E12005, doi:10.1029/2004JE002282.
- Hubbard, W. B., et al. (1993), The occultation of 28 Sgr by Titan, *Astron. Astrophys.*, **269**, 541–563.
- Kostiuk, T., K. E. Fast, T. A. Livengood, T. Hewagama, J. J. Goldstein, F. Espenak, and D. Buhl (2001), Direct measurement of winds on Titan, *Geophys. Res. Lett.*, **28**, 2361–2364.
- Kostiuk, T., T. A. Livengood, T. Hewagama, G. Sonnabend, K. E. Fast, K. Murakawa, A. T. Tokunaga, J. Annen, D. Buhl, and F. Schmüling (2004), Titan's wind and unanticipated temperature asymmetry, abstract astro-ph/0412664, ArXiv, Cornell Univ., Ithaca, N. Y.
- Kostiuk, T., T. A. Livengood, T. Hewagama, G. Sonnabend, K. E. Fast, K. Murakawa, A. T. Tokunaga, J. Annen, D. Buhl, and F. Schmüling (2005), Titan's stratospheric zonal wind, temperature, and ethane abundance a year prior to Huygens insertion, *Geophys. Res. Lett.*, **32**, L22205, doi:10.1029/2005GL023897.
- Kostiuk, T., et al. (2006), Stratospheric global winds on Titan at the time of Huygens descent, *J. Geophys. Res.*, **111**, E07S03, doi:10.1029/2005JE002630.
- Lebreton, J.-P., and D. L. Matson (1997), The Huygens probe: Science, payload and mission overview, in *Huygens: Science, Payload and Mission*, Eur. Space Agency Spec. Publ., ESA SP-1177, 5–24.
- Luz, D., F. Hourdin, P. Rannou, and S. Lebonnois (2003), Latitudinal transport by barotropic waves in Titan's stratosphere: II. Results from a coupled dynamics-microphysics-photochemistry GCM, *Icarus*, **166**, 343–358.
- Luz, D., T. Civeit, R. Courtin, J.-P. Lebreton, D. Gautier, P. Rannou, A. Kaufer, O. Witasse, L. Lara, and F. Ferri (2005), Characterization of zonal winds in the stratosphere of Titan with UVES, *Icarus*, **179**, 497–510.
- Martić, M., J.-C. Lebrun, J. Schmitt, J.-P. Lebreton, and T. Appourchaux (2001), Feasibility demonstration of Titan wind measurement technique at OHP using absolute accelerometry method, technical report, Observ. de Haute Provence, Haute Provence, France.
- Moreno, R., A. Marten, and T. Hidayat (2005), Interferometric measurements of zonal winds on Titan, *Astron. Astrophys.*, **437**, 319–328.
- Porco, C. C., et al. (2005), Imaging of Titan from the Cassini spacecraft, *Nature*, **434**, 159–168.
- Rannou, P., S. Lebonnois, F. Hourdin, and D. Luz (2005), A Titan atmosphere database, *Adv. Space Res.*, **36**, 2194–2198, doi:10.1016/j.asr.2005.09.041.
- Roe, H. G., I. de Pater, B. A. Macintosh, and C. P. McKay (2002), Titan's clouds from Gemini and Keck adaptive optics imaging, *Astrophys. J.*, **581**, 1399–1406, doi:10.1086/344403.
- Sicardy, B., et al. (1990), Probing Titan's atmosphere by stellar occultation, *Nature*, **343**, 350–353.
- Sicardy, B., et al. (2006), The two Titan stellar occultations of 14 November 2003, *J. Geophys. Res.*, doi:10.1029/2005JE002624, in press.
- Wilcoxon, F. (1945), Individual comparisons by ranking methods, *Biometrika*, **1**, 80–83.
- R. Courtin and D. Gautier, Laboratoire d'Etudes Spatiales et d'Instrumentation en Astrophysique (LESIA), Observatoire de Paris, Section de Meudon, 5 Place Jules Janssen, F-92195 Meudon CEDEX, France.
- T. Civeit, J.-P. Lebreton, and O. Witasse, Research and Scientific Support Department of ESA, ESTEC, Keplerlaan 1, P.O. Box 299, NL-2200 AG Noordwijk, Netherlands.
- F. Ferri, CISAS/Università di Padova, Via Venezia 1, I-35131 Padova, Italy.
- A. Kaufer, European Southern Observatory, Alonso de Cordova 3107, Casilla E-19001, Santiago 19, Chile.
- T. Kostiuk and T. Livengood, NASA Goddard Space Flight Center, Greenbelt, MD 20771, USA.
- L. Lara, Instituto de Astrofísica de Andalucía/CSIC, Camino Bajo de Hueter 50, E-18008, Granada, Spain.
- D. Luz, Centro de Astronomia e Astrofísica da Universidade de Lisboa (CAAUL), Observatório Astronómico de Lisboa, Tapada da Ajuda, P-1349-018 Lisboa, Portugal. (dluz@oal.ul.pt)